ELSEVIER

Ceramics International 30 (2004) 2191–2201

CERAMICS INTERNATIONAL

www.elsevier.com/locate/ceramint

Magnetic properties of Y–Fe–O ultrafine particles containing $YFe_{(3+x)}O_{1.5(4+x)}$ synthesized by rf thermal plasma

M. Sugasawa [a,*], N. Kikukawa [a], Y. Nagano [a], N. Kayano [b], T. Kimura [b]

[a] *National Institute of Advanced Industrial Science and Technology, 16-1 Onogawa, Tsukuba, Japan*
[b] *Shibaura Institute of Technology, 3-9-14 Shibaura, Minato, Tokyo, Japan*

Received 18 November 2003; received in revised form 30 December 2003; accepted 29 January 2004
Available online 26 April 2004

Abstract

Y–Fe–O ultrafine particles containing $YFe_{(3+x)}O_{1.5(4+x)}$, ε-Fe_2O_3, and γ-Fe_2O_3(Fe_3O_4) were fabricated using a thermal plasma evaporation method with rf Ar–O_2. To determine if $YFe_{(3+x)}O_{1.5(4+x)}$ in the particles is a ferri-, ferro-, or paramagnetic compound at room temperature (R.T.), the magnetic properties of these particles at R.T. were studied using X-ray diffraction (XRD), vibrating sample magnetometer (VSM), and Mössbauer spectrometry. VSM results showed that the saturation magnetization of particles at R.T. increased after the Curie point (CP) measurement at reduced pressure (4×10^{-3} Pa) from R.T. to an upper limit temperature higher than 460 °C. The saturation magnetization of particles at R.T. after the CP measurement at reduced pressure from R.T. to 700 °C was larger than that from R.T. to 600 °C. In the XRD patterns, the relative quantities of h-$YFeO_3$ and γ-Fe_2O_3(Fe_3O_4) to that of $YFe_{(3+x)}O_{1.5(4+x)}$ increased after the CP measurement at reduced pressure from R.T. to 700 °C, indicating that the saturation magnetization at R.T. increased as the relative quantity of γ-Fe_2O_3(Fe_3O_4) increased. The relative quantities of h-$YFeO_3$ and γ-Fe_2O_3(Fe_3O_4) to that of $YFe_{(3+x)}O_{1.5(4+x)}$ after the CP measurement depended on Fe/Y of the particles, indicating that the increase in saturation magnetization at R.T. after the Curie point measurement depended on the increase in relative quantity of γ-Fe_2O_3(Fe_3O_4). Mössbauer spectrometry before and after the CP measurements showed that $YFe_{(3+x)}O_{1.5(4+x)}$ exhibited only a single type of quadrupole splitting and no magnetic splitting, indicating that $YFe_{(3+x)}O_{1.5(4+x)}$ is a paramagnetic compound.

Keywords: C. Magnetic properties; Thermal plasma

1. Introduction

Yttrium is used in a wide variety of materials. For example, Y_2O_3 is a component in optical glass and is a crystal for the red phosphor used in color televisions that use Eu^{3+} ions as luminescent ions [1]. $YBa_2Cu_3O_x$ is well known as a superconductive material [2]. YAG ($Y_3Al_5O_{12}$: yttrium aluminum garnet) is widely used as a crystalline luminescent element in solid lasers [2]. YIG ($Y_3Fe_5O_{12}$: yttrium iron garnet) containing iron is used as an optical isolator [2]. Broader applications of yttrium by synthesizing new compounds containing yttrium by a thermal plasma evaporation method is expected because new intermediate and metastable compounds are easy to synthesize by this method due to its quenching process.

Ultrafine particles containing $YFe_{(3+x)}O_{1.5(4+x)}$, h-$YFeO_3$, ε-Fe_2O_3, and a spinel-type iron oxide have been synthesized using a thermal plasma evaporation method with a radio frequency induction (rf) Ar–O_2 thermal plasma [3–8]. This spinel-type iron oxide is possibly a non-stoichiometric compound, and will thus be expressed here as γ-Fe_2O_3(Fe_3O_4). $YFe_{(3+x)}O_{1.5(4+x)}$ is a new compound not registered in the PDF database of X-ray diffraction (XRD) patterns of known substances [7–9], is a cubic crystal whose face-centered cubic lattices are formed by metal atoms, and has long-period structure whose maximum peak in its XRD pattern is (444) [9]. Y–Fe–O ultrafine particles containing $YFe_{(3+x)}O_{1.5(4+x)}$ synthesized by the thermal plasma evaporation method contain ferri- or ferromagnetic compounds at room temperature (R.T.) [8,9]. γ-Fe_2O_3(Fe_3O_4) identified by XRD in these particles significantly increases the saturation magnetization at R.T. [8].

In this study, to determine if $YFe_{(3+x)}O_{1.5(4+x)}$ is a ferri-, ferro-, or paramagnetic compound, we studied the

* Corresponding author.
E-mail address: m-sugasawa@aist.go.jp (M. Sugasawa).

0272-8842/$30.00 © 2004 Elsevier Ltd and Techna S.r.l. All rights reserved.
doi:10.1016/j.ceramint.2004.01.003

magnetic properties of Y–Fe–O ultrafine particles containing $YFe_{(3+x)}O_{1.5(4+x)}$ by using XRD to identify the Y–Fe–O compounds, vibrating sample magnetometer (VSM) to measure the saturation magnetization and Curie point (CP), and Mössbauer spectrometry to measure the magnetization properties of the particles.

2. Experimental

Fig. 1 shows a schematic of the rf thermal plasma reactor used to synthesize Y–Fe–O ultrafine particles containing $YFe_{(3+x)}O_{1.5(4+x)}$ [8]. The plasma torch was composed of a water-cooled double quartz tube, a copper bulkhead, a copper probe, and a three-turn rf coil. The rf coil was connected to an rf power supply that had a maximum plate power of 60 kW and a frequency of 4 MHz. The bulkhead and probe were installed in the upper part of the plasma torch. Plasma gas (A) was introduced into the torch via a gap between the bulkhead and probe and had a swirl component. Sheath gas (B) was introduced in the radial direction from the outer surface of the bulkhead and had no swirl component. Sheath gas (C) was introduced in the tangential direction of the outer surface of the bulkhead and had a swirl component. The locations of A, B, and C prevented cooling of the skin region generating eddy currents that supplied the plasma with thermal energy. The swirl components of A and C kept the eddy flow peculiar to rf thermal plasma away from the plasma central axis. The result was a more stable plasma torch than torches whose gas inlets are annular quartz tubes [10]. Precursor and carrier gases (D) were introduced at the end of the probe. In this study, rf Ar–O_2 thermal plasma at atmospheric pressure was used in the synthesis because the objective was a product that was an oxide. O_2 gas was used as the one of the sheath gases B or C, and Ar gas was used as the plasma gas A, and as the other sheath gas B or C, and as the carrier gas D. Amorphous citrate gel powder was used as the precursor, with a constant Fe/Y ratio (dimensionless: molar ratio) and particle diameter (<45 μm) [4].

Because the products contained in particles depend on the collection locations [3,6], the particles were collected (by using a brush) at five specific locations in the downstream of the plasma torch: the inlet port of the quenching gas (QP), the upper surface of quartz board (QB), Pyrex tube (PT), the side inner wall and ceiling board of the collection chamber (S), and filter (F). The mass of the particles collected at these respective locations was M_{QP}, M_{QB}, M_{PT}, M_S, and M_F. No quenching gas was used in this study because a plasma tail flame that is kept long was suitable for the synthesis of $YFe_{(3+x)}O_{1.5(4+x)}$. The vertical distance between QB and S could be adjusted by moving QB vertically. In this study, the vertical distance was 450 mm during particle synthesis.

Table 1 lists the synthesis conditions for five different values of Fe/Y. The value of Fe/Y was measured

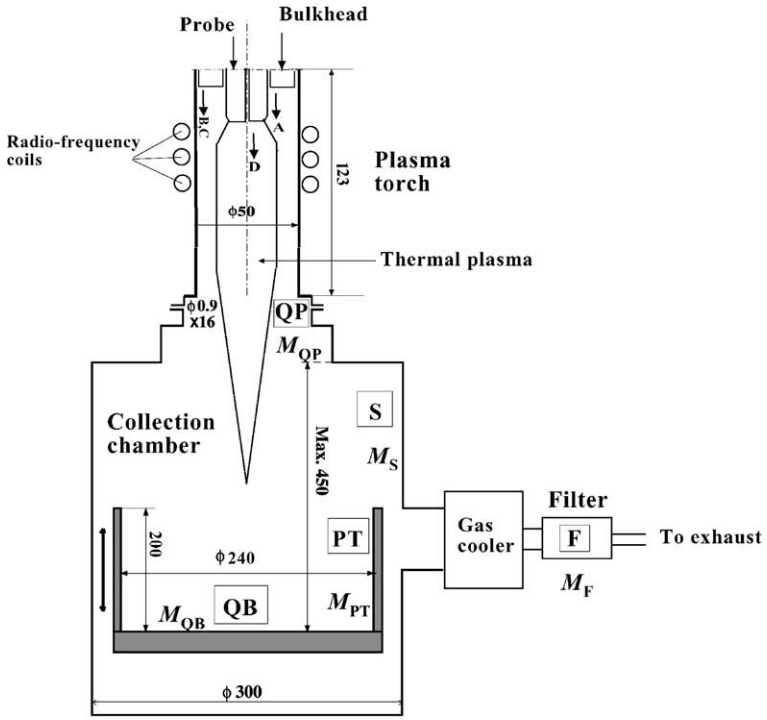

Fig. 1. Experimental apparatus to synthesize Y–Fe–O ultrafine particles containing $YFe_{(3+x)}O_{1.5(4+x)}$ by rf thermal plasma (dimensions are in millimeters). A: plasma gas (with swirl); B: sheath gas (without swirl); C: sheath gas (with swirl); D: precursor + carrier gas; M_{QP}: mass of particles collected at QP; M_{QB}: mass of particles collected at QB; M_{PT}: mass of particles collected at PT; M_S: mass of particles collected at S; M_F: mass of particles collected at F; QP: quenching port; QB: quartz board; PT: Pyrex tube; S: side wall; F: filter.

Table 1
Experimental conditions in the synthesis of Y–Fe–O ultrafine particles containing $YFe_{(3+x)}O_{1.5(4+x)}$ by rf thermal plasma

	Run number				
	E503	E403	E408	E405	E406
Fe/Y (-; molar ratio): product	2.7	2.9	3.3	3.5	4.0
A(Ar): plasma gas (m^3/s)	2.3×10^{-4}	2.5×10^{-4}	2.3×10^{-4}	2.3×10^{-4}	2.3×10^{-4}
B(Ar): sheath gas (m^3/s)	3.7×10^{-4}	3.7×10^{-4}	3.5×10^{-4}	3.8×10^{-4}	3.7×10^{-4}
B(O_2): sheath gas (m^3/s)	1.0×10^{-4}	1.0×10^{-4}	1.0×10^{-4}	1.0×10^{-4}	1.0×10^{-4}
C(Ar): sheath gas (m^3/s)	3.8×10^{-4}	3.7×10^{-4}	3.8×10^{-4}	4.2×10^{-4}	3.8×10^{-4}
C(O_2): sheath gas (m^3/s)	2.0×10^{-4}	2.0×10^{-4}	2.0×10^{-4}	2.0×10^{-4}	2.0×10^{-4}
D(Ar): carrier gas (m^3/s)	5.0×10^{-5}	5.0×10^{-5}	5.0×10^{-5}	5.0×10^{-5}	5.0×10^{-5}
Plate power (kW)	33.6	25.9	30.0	23.8	24.5
Feed time (s)	1.6×10^{3}	9.6×10^{2}	7.2×10^{2}	1.7×10^{3}	2.3×10^{3}
Feed quantity (kg)	5.1×10^{-3}	4.9×10^{-3}	6.7×10^{-3}	9.7×10^{-3}	2.1×10^{-2}
Feed rate (kg/s)	3.2×10^{-6}	5.0×10^{-6}	9.3×10^{-6}	5.8×10^{-6}	9.5×10^{-6}

using inductively coupled plasma emission spectroscopy (ICP-ES).

For all five runs, the total gas volumetric flow rate was relatively constant. The plate power was adjusted to maintain stable plasma operation. However, the precursor flow caused the plasma to become unstable, which made it difficult to maintain the feed rate over all runs. Therefore, maintaining a constant feed rate of the precursor was not possible.

XRD was used to identify the synthesized products in the ultrafine particles. ICP-ES was used to measure the Fe/Y of the particles. VSM was used to measure the CP for the particles in which $YFe_{(3+x)}O_{1.5(4+x)}$ apparently existed close to pure single phase from R.T. to 600 °C, namely, run S E405 (Fe/Y = 3.5) based on the XRD pattern. In VSM, first a magnetized sample was vibrated with a sinusoidal wave in which both the amplitude and frequency were constant, and then the magnetization generated by the direct current from the electromotive force induced in a coil placed 14 mm from the particles was measured. In the CP measurement, a magnetic field of 2.0×10^5 A/m was applied, and heating was immediately stopped as soon as the temperature of the particles reached 600 °C, and thus the particles were cooled gradually. The measurement was done under reduced pressure (4×10^{-3} Pa) to prevent oxidation caused by the high temperature. While the temperature was increased to 600 °C, the saturation magnetization of the particles unnaturally showed maximum and minimum values, suggesting that the particles were undergoing chemical reactions that were reduction reactions caused by the reduced pressure (see Fig. 3). Therefore, to suppress these chemical reactions, CP measurements were also done under atmospheric pressure (10^5 Pa). To determine these chemical reactions, CP measurements were done from R.T. to three temperatures (230, 340, and 460 °C) existing between the two maximum points above which the saturation magnetization value began to increase from R.T. to 600 °C by VSM (see Fig. 3). To promote these chemical reactions, CP measurements were also done at reduced temperature (4×10^{-3} Pa) from R.T to 700 °C for particles collected at location S for the individual runs shown in Table 1 by VSM.

XRD was used to identify the compounds in the particles before and after the CP measurements at reduced pressure of 4×10^{-3} Pa (hereafter called RP) from R.T. to 230 °C (hereafter called RP/RT/230), from R.T. to 340 °C (RP/RT/340), from R.T. to 460 °C (RP/RT/460), and from R.T. to 600 °C (RP/RT/600), and at atmospheric pressure of 10^5 Pa (hereafter called AP) from R.T. to 600 °C (AP/RT/600). To determine the effect of CP measurement on the type and relative quantities of Y–Fe–O compounds in the particles, XRD patterns of the particles before and after the CP measurements were compared. VSM was also used to measure the saturation magnetization of these particles at R.T. To determine the effect of Fe/Y in the particles on saturation magnetization at R.T., VSM of the particles of different Fe/Y were compared. Transmission electron microscopy (TEM) was used to observe these particles before and after CP measurements.

Mössbauer spectrometry was used to measure the magnetic properties of the Y–Fe–O ultrafine particles before and after CP measurements (RP/RT/600 and RP/RT/700) to determine if $YFe_{(3+x)}O_{1.5(4+x)}$ is a ferri-, ferro-, or paramagnetic compound.

3. Results and discussion

3.1. Mass of collected particles

Table 2 shows the mass of particles collected at different locations for five runs. Increasing the mass flow of the precursor did not necessarily increase the total collection mass ($M_{total} = M_{QP} + M_{QB} + M_{PT} + M_S + M_F$) of the particles. However, Run E406 (Fe/Y = 4.0) had the highest precursor mass flow, highest M_S, and highest M_F. For all five runs, M_S and M_F were higher than the mass collected at the other locations (i.e. M_{QP}, M_{QB}, and M_{PT}).

3.2. Identification of compounds in the synthesized particles revealed by XRD

Fig. 2 shows the XRD patterns of the particles collected at location S for the five runs. For all runs, the synthe-

Table 2
Mass of particles collected particles at different locations for five runs

	Run number				
	E503	E403	E408	E405	E406
M_{QP} (kg)	8.00×10^{-6}	2.00×10^{-5}	3.10×10^{-5}	5.40×10^{-5}	1.29×10^{-4}
M_{QB} (kg)	8.00×10^{-6}	2.00×10^{-6}	6.00×10^{-6}	4.00×10^{-6}	4.00×10^{-6}
M_{PT} (kg)	1.38×10^{-4}	2.00×10^{-6}	7.40×10^{-5}	1.00×10^{-6}	–
M_S (kg)	2.81×10^{-4}	3.34×10^{-4}	5.11×10^{-4}	9.02×10^{-4}	2.33×10^{-3}
M_F (kg)	3.06×10^{-4}	9.44×10^{-4}	3.08×10^{-4}	5.34×10^{-4}	1.16×10^{-3}
M_{total}[a] (kg)	7.41×10^{-4}	1.30×10^{-3}	9.30×10^{-4}	1.50×10^{-3}	3.62×10^{-3}

[a] $M_{total}=M_{QP}+M_{QB}+M_{PT}+M_S+M_F$.

sized particles contained $YFe_{(3+x)}O_{1.5(4+x)}$, h-$YFeO_3$, γ-Fe_2O_3(Fe_3O_4), and ε-Fe_2O_3 [11–13]. γ-Fe_2O_3(Fe_3O_4) and ε-Fe_2O_3 are ferrimagnetic compounds at R.T. [14]. For Run E406 (Fe/Y = 4.0), the XRD pattern shows seven peaks: the main four peaks (444), (800), (880), and (1244) of $YFe_{(3+x)}O_{1.5(4+x)}$, the maximum peak (102) of h-$YFeO_3$, the maximum peak (311) of γ-Fe_2O_3(Fe_3O_4), and the maximum peak (122) of ε-Fe_2O_3.

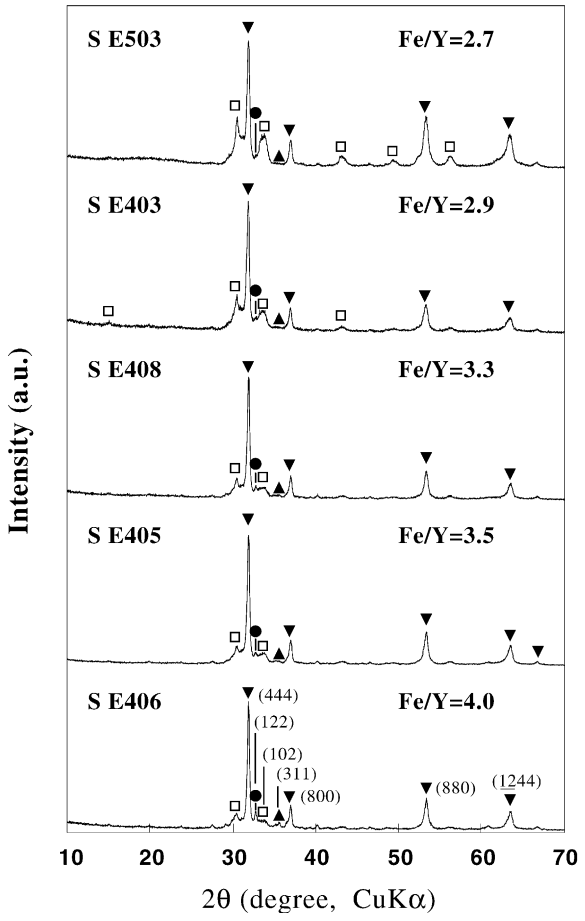

Fig. 2. XRD patterns for particles collected at location S to identify Y–Fe–O compounds in particles with different Fe/Y ratio. (▼) $YFe_{(3+x)}O_{1.5(4+x)}$; (□) h-$YFeO_3$; (▲) γ-Fe_2O_3(Fe_3O_4); (●) ε-Fe_2O_3.

3.3. Effect of CP measurement on XRD pattern and saturation magnetization of particles at R.T.

Fig. 3 shows the results of the CP measurements at RP/RT/600 and AP/RT/600 for particles collected at location S for Run E405 (Fe/Y = 3.5). At RP, the saturation magnetization unnaturally showed local maxima and minima as the temperature increased, suggesting that the particles were undergoing chemical reactions that were reduction reactions caused by the reduced pressure. To suppress these chemical reactions, CP measurements were also done under AP. At AP, although a local maximum occurred at around 200 °C and the degree of decrease in the saturation magnetization changed at around 380 °C, overall the saturation magnetization decreased.

Fig. 4 shows the XRD patterns of particles collected at S for Run E405 before and after the CP measurements at RP/RT/230, RP/RT/340, RP/RT/460, and RP/RT/600. The XRD pattern of particles after the CP measurement at RP/RT/230 clearly shows the maximum peak (122) of ε-Fe_2O_3. This peak was absent in the pattern for particles after the CP measurement at RP/RT/340. Therefore, ε-Fe_2O_3 disappeared between 230 and 340 °C. The maximum peak (311) of γ-Fe_2O_3 (Fe_3O_4) for the particles after the CP measurement at RP/RT/600 was larger than that at RP/RT/460, indicating that the relative quantity of γ-Fe_2O_3(Fe_3O_4) increased between 460 and 600 °C due to chemical reactions.

Fig. 5 shows the XRD patterns of particles collected at S for Run E405 before and after the CP measurement at AP/RT/600. The XRD pattern of the particles after the CP measurement clearly show the main four peaks of $YFe_{(3+x)}O_{1.5(4+x)}$, the peaks of cubic (c-)Cu_2O [15], and those of monoclinic (m-)CuO [16]. c-Cu_2O and m-CuO apparently were mixed into the particles as impurities due to the oxidation of Cu in the Cu sample holder during the CP measurement. This oxidation was caused by the high oxygen partial pressure due to AP.

Fig. 6 shows the saturation magnetization of particles at R.T. before and after the CP measurements as a function of upper limit temperatures of the CP measurements at RP and AP. The value of the particles before the CP measurement

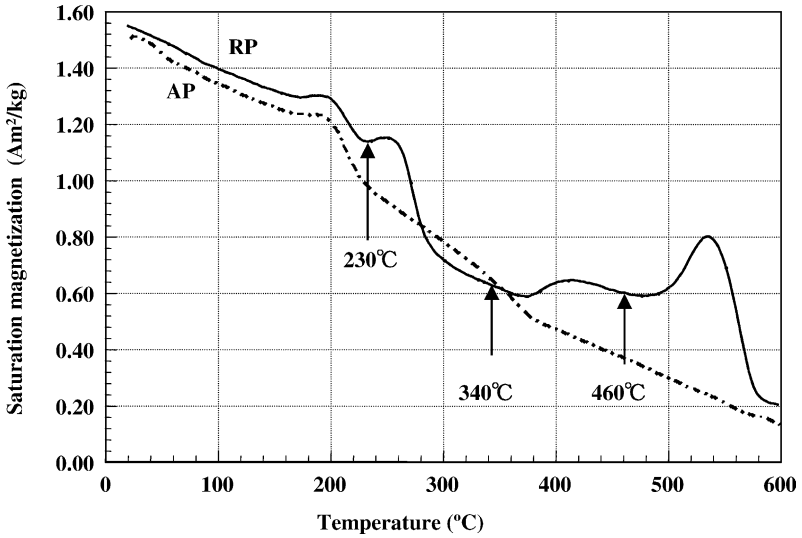

Fig. 3. Saturation magnetization of particles collected at location S for Run E405 (Fe/Y = 3.5) vs. temperature. RP: Curie point measurement at reduced pressure (4×10^{-3} Pa); AP: Curie point measurement at atmospheric pressure (10^5 Pa).

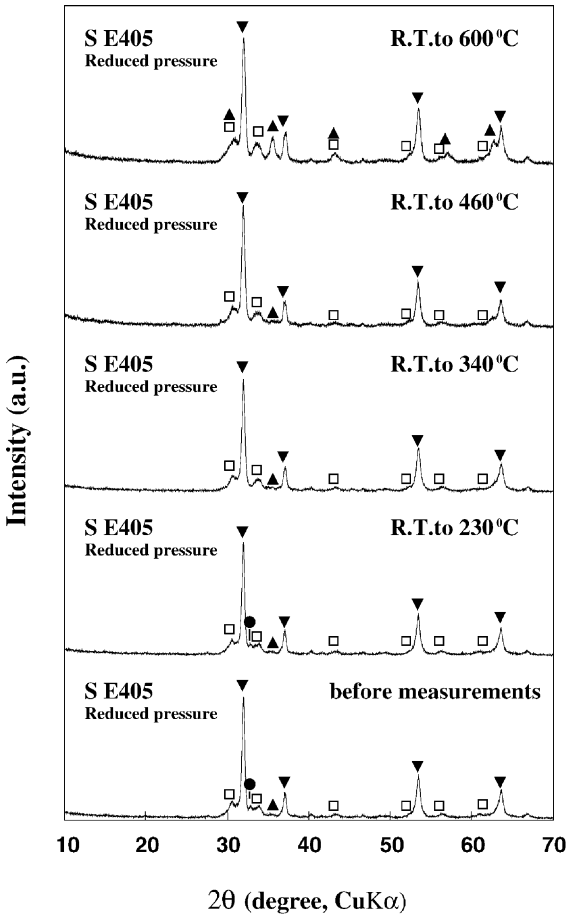

Fig. 4. XRD patterns for particles collected at location S for Run E405 (Fe/Y = 3.5) before and after Curie point measurements at reduced pressure (4×10^{-3} Pa). (▼) $YFe_{(3+x)}O_{1.5(4+x)}$; (□) h-$YFeO_3$; (▲) γ-Fe_2O_3(Fe_3O_4); (●) ε-Fe_2O_3.

was plotted against R.T. The saturation magnetization at RP/RT/230 was slightly larger than that at RP/RT/340 and RP/RT/460. Because the maximum saturation magnetization at 230 °C was larger than that at R.T. (for particles containing ε-Fe_2O_3 before the CP measurement), it is impossible to relate the maximum value at 230 °C with the disappearance of ε-Fe_2O_3 between 230 and 340 °C. In the XRD patterns (Fig. 4), no peak ascribed to any ferri- or ferromagnetic compounds except for ε-Fe_2O_3 and γ-Fe_2O_3(Fe_3O_4) appeared for particles after the CP measurement at RP/RT/230, or for particles before and after the CP measurement at RP/RT/340. Therefore, the maximum value at 230 °C can be regarded as within experimental error. On the other hand, the value at RP/RT/600 was about

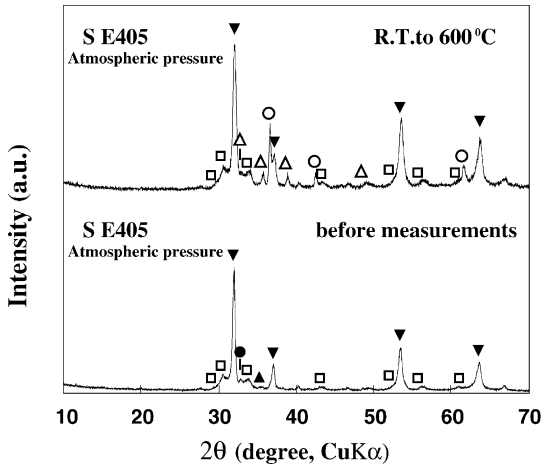

Fig. 5. XRD patterns for particles collected at location S for Run E405 (Fe/Y = 3.5) before and after Curie point measurements at atmospheric pressure (10^5 Pa). (▼) $YFe_{(3+x)}O_{1.5(4+x)}$; (□) h-$YFeO_3$; (▲) γ-Fe_2O_3(Fe_3O_4); (●) ε-Fe_2O_3; (○) c-Cu_2O; (△) m-CuO.

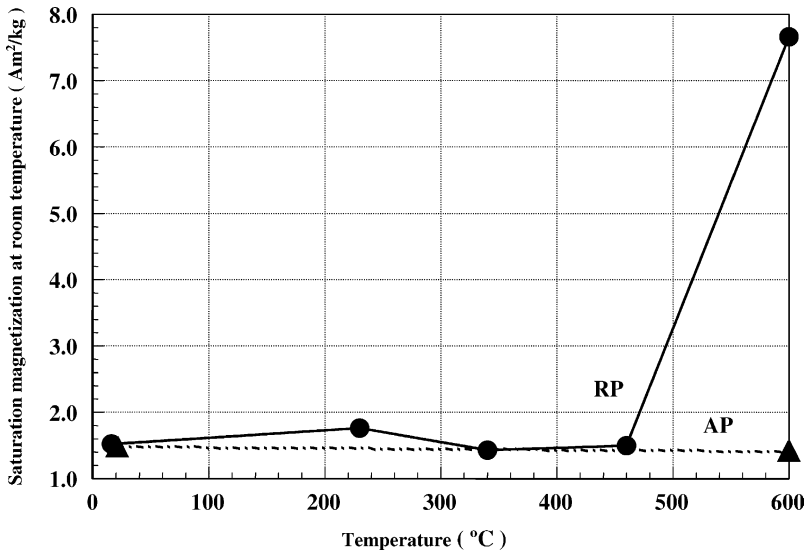

Fig. 6. Saturation magnetization at room temperature for particles collected at location S for Run E405 (Fe/Y = 3.5) before and after Curie point measurements. RP: Curie point measurements at reduced pressure (4×10^{-3} Pa); AP: Curie point measurements at atmospheric pressure (10^5 Pa).

five times larger than that at RP/RT/460, indicating that the relative quantity of γ-Fe_2O_3(Fe_3O_4) in the particles increased due to the above-mentioned chemical reaction between 460 and 600 °C (see Fig. 4). However, at AP, the relative quantity at 600 °C was almost the same as that at R.T. Although c-Cu_2O and m-CuO were mixed into the particles as impurities, they were paramagnetic compounds at R.T. At AP, however, the relative quantity of γ-Fe_2O_3 (Fe_3O_4) in the particles did not increase (Fig. 5). Taken together, these results show that at AP the XRD pattern of the particles remained unchanged after the CP measurement except for the change caused by the mixture of c-Cu_2O and m-CuO as impurities.

Fig. 7 shows TEM photographs of particles whose XRD patterns are shown in Fig. 4 before and after the CP measurements at RP/RT/230, RP/RT/340, RP/RT/460, and RP/RT/600. The average particle diameter did not increase even when the upper limit temperature of the CP measurement increased. Fig. 7e shows a TEM photograph of the particles after the measurement at RP/RT/600. Although the saturation magnetization at RP/RT/600 was about five times larger than that after the measurement at RP/RT/460 (see Fig. 6), the degree of agglomeration of the primary particles remained unchanged compared with the particles before and after the measurements at RP/RT/230, RP/RT/340, and RP/RT/460.

Fig. 8 shows the TEM photographs of particles whose XRD patterns are shown in Fig. 5 before and after the CP measurement at AP/RT/600. In the particles after the measurement (Fig. 8b), c-Cu_2O and m-CuO were mixed as impurities. However, comparison between Fig. 8a and b reveals no significant difference in particle diameter distribution or in particle morphology, clearly indicating that the mixture of these impurities did not affect either the particle diameter distribution or particle morphology.

3.4. Effect of Fe/Y in the particles on XRD pattern and saturation magnetization at R.T. after CP measurements

Fig. 9 shows the XRD patterns of particles collected at location S for the five different Fe/Y ratios after the CP measurements at RP/RT/700. (The XRD patterns of the particles before the CP measurements are shown in Fig. 2.) As discussed in Section 3.3, when the CP measurement was done for particles collected at location S for Run E405 (Fe/Y = 3.5) at RP/RT/600, a chemical reaction caused an increase in the relative quantity of γ-Fe_2O_3(Fe_3O_4) in the particles (based on the XRD pattern). Therefore, to promote this chemical reaction, CP measurements were also done at RP/RT/700. Comparison of XRD patterns before (Fig. 2) and after (Fig. 9) the CP measurement reveals that the measurement caused a decrease in the peak intensity of $YFe_{(3+x)}O_{1.5(4+x)}$ and an increase in the peak intensities of h-$YFeO_3$ and γ-Fe_2O_3(Fe_3O_4). Comparison of the XRD pattern of particles collected at location S for Run E405 after the CP measurement at RP/RT/600 (Fig. 4) and that at RP/RT/700 (Fig. 9) reveals that the higher temperature caused a decrease in the relative peak intensities of h-$YFeO_3$ and γ-Fe_2O_3(Fe_3O_4) to that of $YFe_{(3+x)}O_{1.5(4+x)}$. Therefore, the higher temperature of 700 °C promoted the chemical reaction better than did 600 °C, which is the upper limit temperature of the CP measurement.

Fig. 9 also shows that the relative peak intensities of h-$YFeO_3$ and γ-Fe_2O_3(Fe_3O_4) to those of $YFe_{(3+x)}O_{1.5(4+x)}$ depended on Fe/Y. For clarity in the following discussion, we call the peak intensity of the maximum peak (102) of h-$YFeO_3$ in the XRD pattern shown in Fig. 2 as I_1, that of the maximum peak (444) of $YFe_{(3+x)}O_{1.5(4+x)}$ as I_2, that of the maximum peak (122) of ε-Fe_2O_3 as I_3, and that of the maximum peak (3 1 1) of γ-Fe_2O_3(Fe_3O_4) as I_4. Fig. 10a

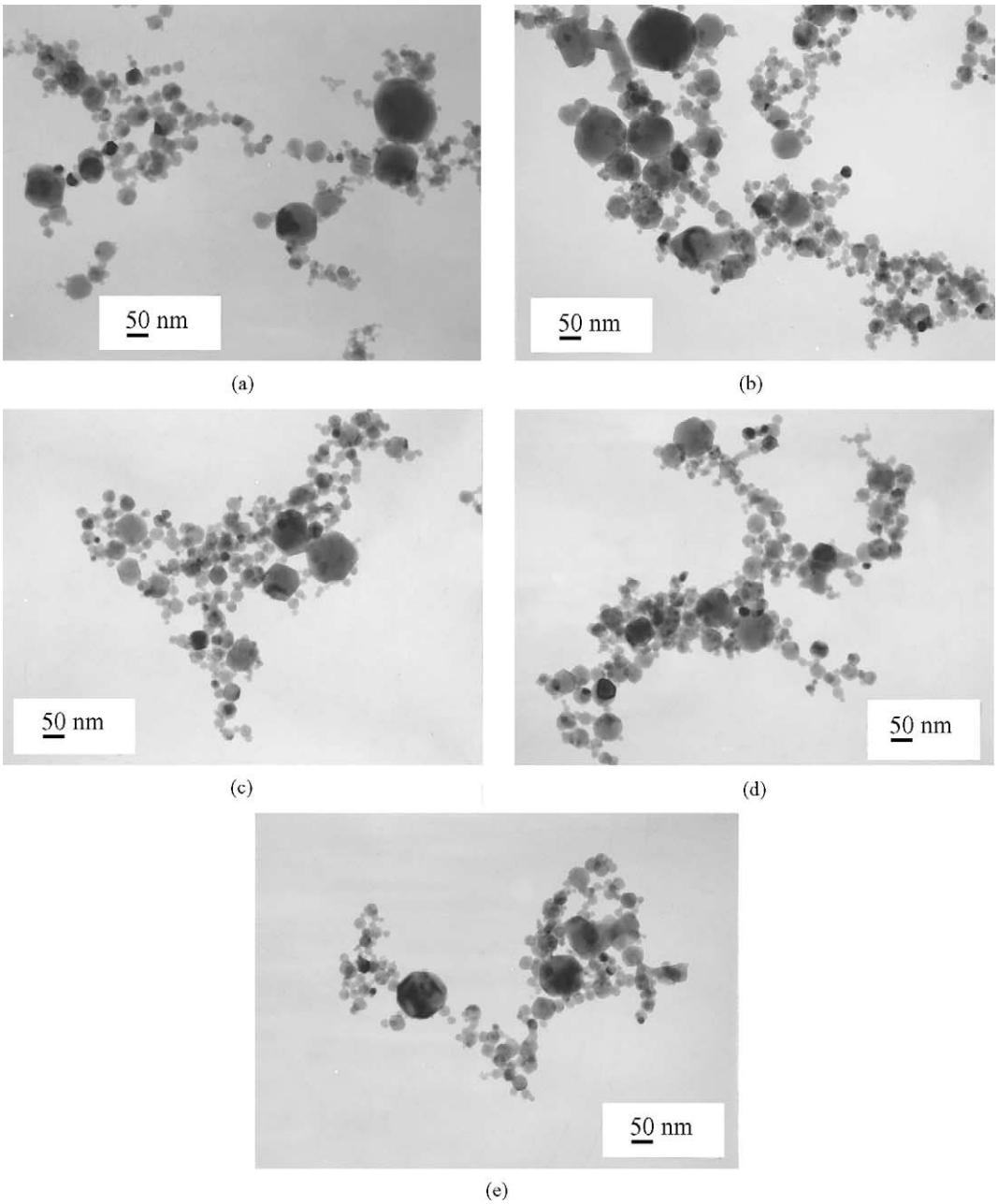

Fig. 7. TEM images of particles collected at location S for Run E405 (Fe/Y = 3.5) (a) before and (b) after Curie point measurement from R.T. to 230 °C, (c) from R.T. to 340 °C, (d) from R.T. to 460 °C, and (e) from R.T. to 600 °C at reduced pressure (4×10^{-3} Pa).

shows the effect of Fe/Y of the particles on I_1/I_2, I_3/I_2, and I_4/I_2 of the particles before the CP measurements. As Fe/Y increased, I_1/I_2 decreased, whereas I_3/I_2 and I_4/I_2 increased. Fig. 10b shows the effect of Fe/Y on I_1/I_2 and I_4/I_2 after the CP measurements. (Because I_3 could not be identified on the XRD patterns in Fig. 9, I_3/I_2 was not plotted in Fig. 10b.) Except for $I_1/I_2 = 0.12$ for Fe/Y = 4.0, all I_1/I_2 and I_4/I_2 were larger than 0.20, indicating that I_1/I_2 and I_4/I_2 increased after the CP measurements. The maximum I_1/I_2 (=4.6) and I_4/I_2 (=6.1) occurred at Fe/Y = 2.9. These results reveal that the relative quantities of h-YFe_2O_3 and γ-Fe_2O_3(Fe_3O_4) to that of $YFe_{(3+x)}O_{1.5(4+x)}$ (in the XRD pattern) increased after the CP measurements at RP/RT/700 and that the relative quantity ratios depended on Fe/Y of the particles.

Fig. 11 shows the effect of Fe/Y of the particles on the saturation magnetization at R.T. of particles before and after the CP measurements at RP/RT/700. Before the CP measurement (Fig. 11a), as Fe/Y increased, the saturation magnetization increased. Furthermore, the magnetization after the CP measurement (Fig. 11b) was significantly higher than that before the measurement. The maximum saturation magnetization (29.7 Am^2/kg) occurred at Fe/Y = 2.9, possibly related to the maximum of I_4/I_2 also occurring at Fe/Y =

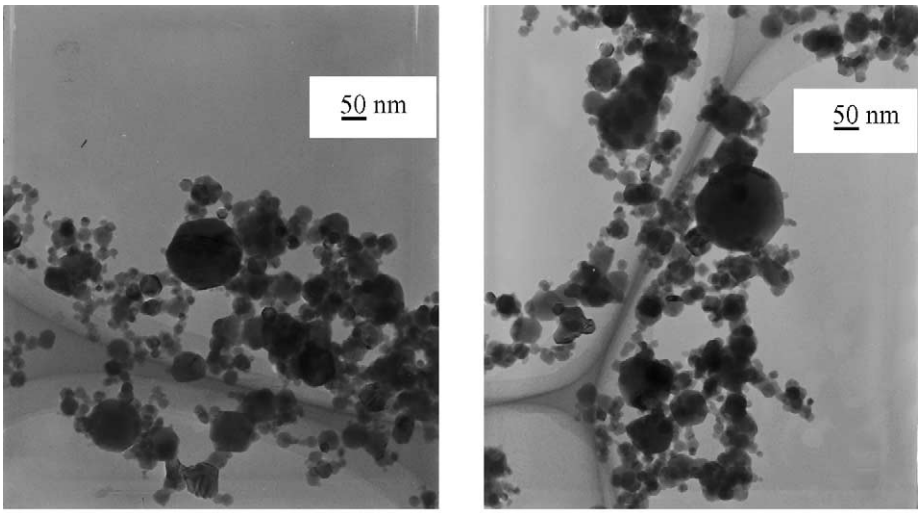

Fig. 8. TEM image of particles collected at location S for Run E405 (Fe/Y = 3.5) (a) before and (b) after Curie point measurement from R.T. to 600 °C at atmospheric pressure (10^5 Pa).

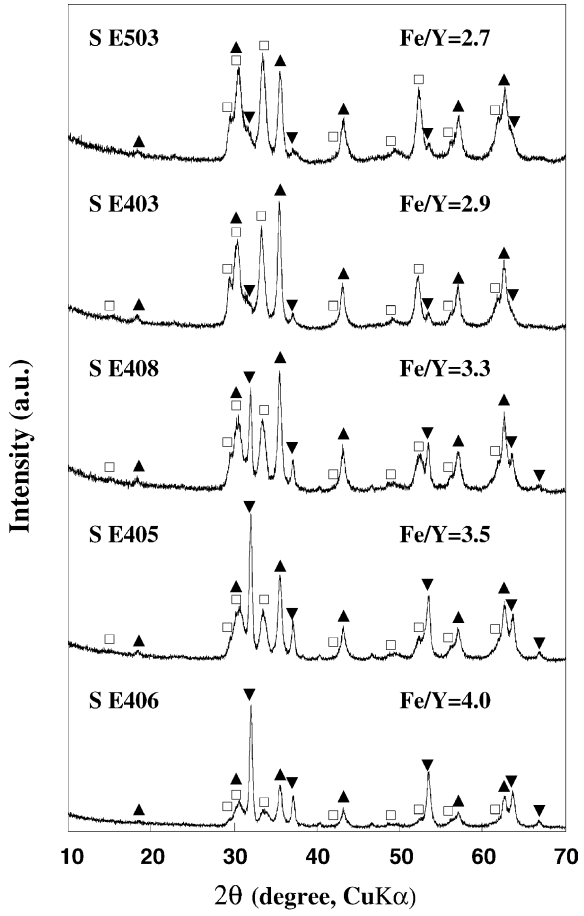

Fig. 9. XRD patterns for particles collected at location S to identify Y–Fe–O compounds in particles after Curie point measurement from R.T. to 700 °C at reduced pressure (4×10^{-3} Pa). (▼) $YFe_{(3+x)}O_{1.5(4+x)}$; (□) h-$YFeO_3$; (▲) γ-Fe_2O_3(Fe_3O_4).

2.9 (Fig. 10b). After the CP measurements, for Fe/Y = 2.9 where the relative quantity of γ-Fe_2O_3 (Fe_3O_4) to that of $YFe_{(3+x)}O_{1.5(4+x)}$ was maximum, the saturation magnetization of the particles at R.T. was also maximum. Therefore, the saturation magnetization after the CP measurements was affected by the relative quantity of γ-Fe_2O_3 (Fe_3O_4) of the particles (XRD pattern) being increased by the chemical reaction during the CP measurement.

3.5. Mössbauer spectrometry analysis of the magnetic properties of Y–Fe–O ultrafine particles containing $YFe_{(3+x)}O_{1.5(4+x)}$ before and after CP measurements

Fig. 12 shows the Mössbauer spectra of particles collected at location S for Run E405 (Fe/Y = 3.5) before and after the CP measurement at RP/RT/600. Table 3 lists the Mössbauer parameters obtained by dividing the individual spectra into Lorenz functions. The column *Area* indicates the peak area ratio, *IS* is the isomer shift, *QS* is

Table 3
Mössbauer parameters of particles collected at location S for Run E405 (Fe/Y = 3.5) before and after Curie point measurement from R.T. to 600 °C at reduced pressure (4×10^{-3} Pa)

Sample	*Partial*	*Area* (%)	*IS* (mm/s)	*QS* (mm/s)	*IF* (T)
S E405	1	54.3	0.35	0.85	–
	2	29.2	0.32	1.59	–
	3	8.8	0.33	−0.04	44.8
	4	5.1	0.41	0.04	39.0
	5	2.6	0.16	0.25	27.9
S E405 (R.T. to 600 °C)	1	63.0	0.34	0.79	–
	2	17.0	0.34	1.81	–
	3	20.0	0.73	0.16	44.6

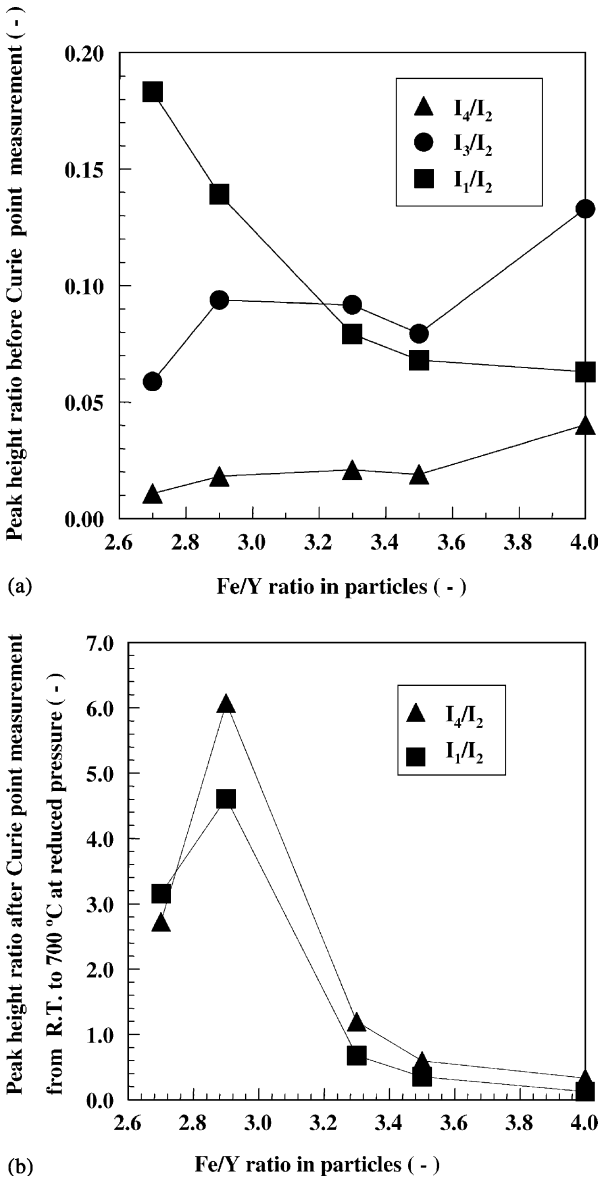

Fig. 10. Peak height ratio vs. Fe/Y ratio in particles (a) before and (b) after Curie point measurement from R.T. to 700 °C at reduced pressure (4×10^{-3} Pa). I_1: peak height of h-$YFeO_3$ (102); I_2: peak height of $YFe_{(3+x)}O_{1.5(4+x)}$ (444); I_3: peak height of ε-Fe_2O_3 (122); I_4: peak height of γ-Fe_2O_3(Fe_3O_4) (311).

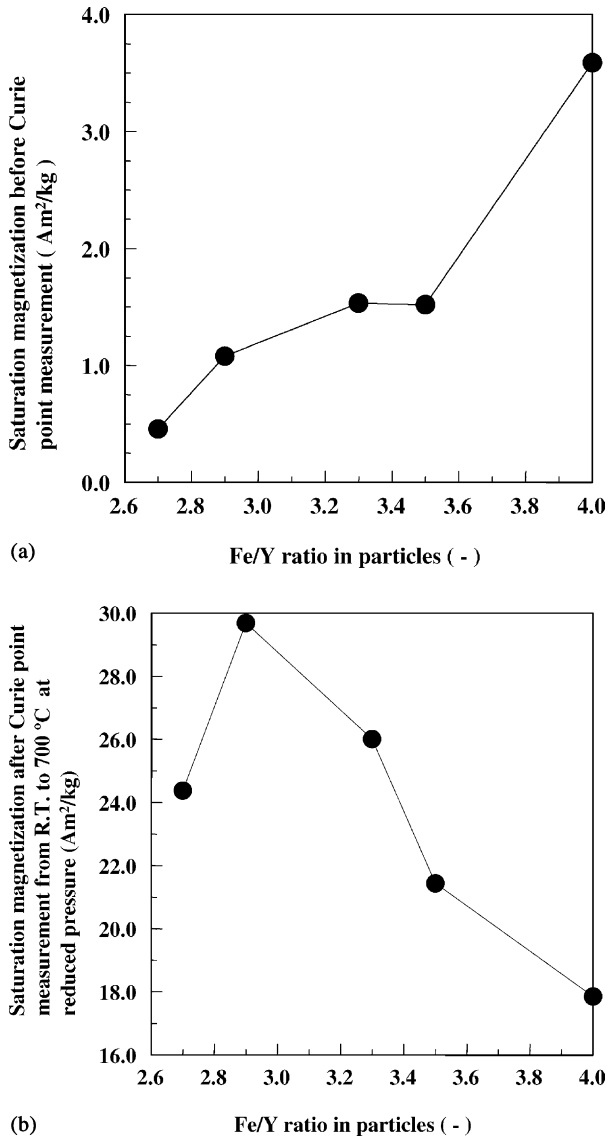

Fig. 11. Saturation magnetization at room temperature for particles collected at location S vs. Fe/Y ratio in particles (a) before and (b) after Curie point measurement from R.T. to 700 °C at reduced pressure (4×10^{-3} Pa).

the width of the quadrupole splitting, and *IF* is the internal magnetic field strength. The spectrum of the particles before the CP measurement (Fig. 12a) showed two types of quadrupole splitting and three types of magnetic splitting. Because the magnetic splitting could be divided into three Lorenz functions, it correspond to plural ferri- or ferromagnetic compounds. The spectrum of the particles after the CP measurement (Fig. 12b) also exhibited two types of quadrupole splitting and one type of magnetic splitting. The magnetic splitting could not be divided into plural Lorenz functions due to significant noise in the spectrum. Assuming that a single type of the quadrupole splitting corresponds to a paramagnetic compound in Fig. 12a, the particles before the CP measurement contained two paramagnetic and plural ferri- or ferromagnetic compounds. In the XRD pattern of the particles before the CP measurement (Fig. 2), $YFe_{(3+x)}O_{1.5(4+x)}$ apparently existed as nearly pure single phase along with the other products, such as h-$YFeO_3$, γ-Fe_2O_3(Fe_3O_4), and ε-Fe_2O_3. The saturation magnetization of the particles at R.T. before the CP measurement was 1.52 Am^2/kg (Fig. 11a). However, the particles after the CP measurement contained $YFe_{(3+x)}O_{1.5(4+x)}$, h-$YFeO_3$, and γ-Fe_2O_3(Fe_3O_4), but not ε-Fe_2O_3 (Fig. 4). The saturation magnetization of the particles at R.T. after the CP measurement was 7.66 Am^2/kg (Fig. 6). Because the particles before the measurement contained γ-Fe_2O_3(Fe_3O_4) and ε-Fe_2O_3, these compounds probably correspond to the magnetic splitting evident in Fig. 12a. In contrast, the particles after the CP

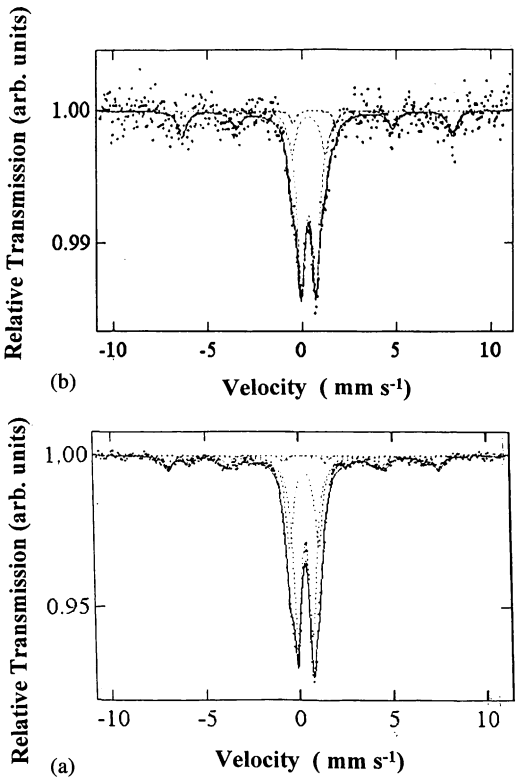

Fig. 12. Mössbauer spectra for particles collected at location S for Run E405 (Fe/Y = 3.5) (a) before and (b) after Curie point measurement from R.T. to 600 °C at reduced pressure (4×10^{-3} Pa).

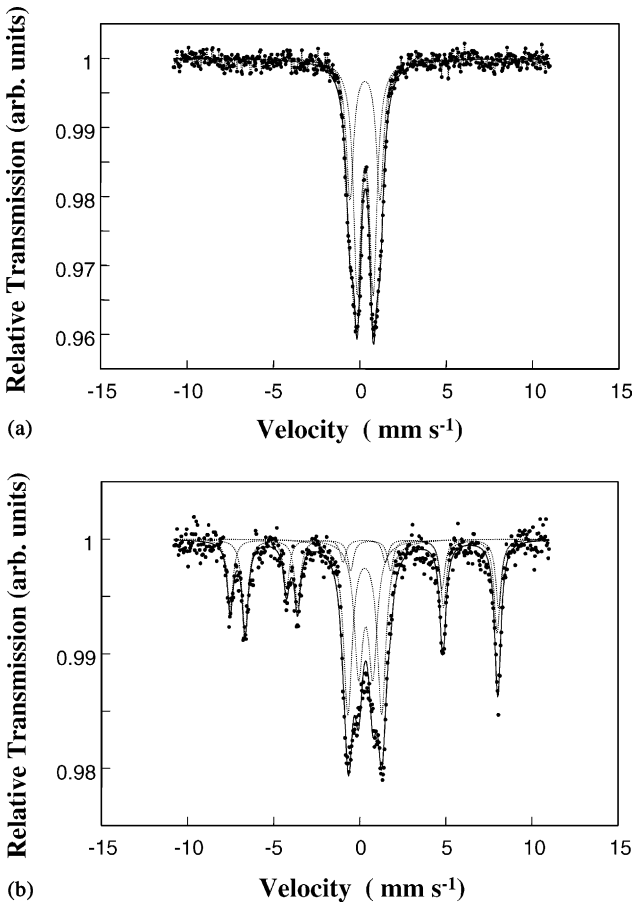

Fig. 13. Mössbauer spectra for particles collected at location S for Run E503 (Fe/Y = 2.7) (a) before and (b) after Curie point measurement from R.T. 700 °C at reduced pressure (4×10^{-3} Pa).

measurement (Fig. 12b) contained two paramagnetic compounds and at least one ferri- or ferromagnetic compound. Because the relative quantity of γ-Fe_2O_3(Fe_3O_4) of the particles after the CP measurement increased (XRD pattern in Fig. 4), γ-Fe_2O_3(Fe_3O_4) corresponds to the magnetic splitting evident in Fig. 12b. On the other hand, one of two types of quadrupole splitting (*QS* in Table 3) seen in the spectrum both before (Fig. 12a) and after (Fig. 12b) the CP measurement corresponds to h-$YFeO_3$, which is a paramagnetic compound.

Fig. 13 shows the Mössbauer spectra for particles collected at location S for Run E503 (Fe/Y = 2.7) before and after the CP measurement at RP/RT/700. Table 4 lists

Table 4
Mössbauer parameters of particles collected at location S for Run E503 (Fe/Y = 2.7) before and after Curie point measurement from R.T. to 700 °C at reduced pressure (4×10^{-3} Pa)

Sample	*Partial*	*Area* (%)	*IS* (mm/s)	*QS* (mm/s)	*IF* (T)
S E503	1	61.4	0.32	0.92	–
	2	38.6	0.30	1.74	–
S E503 (R.T. to 700 °C)	1	24.0	0.36	0.83	–
	2	32.4	0.31	1.96	–
	3	18.5	0.28	0.01	48.4
	4	25.1	0.66	0.04	45.5

the Mössbauer parameters obtained by dividing the individual spectra into Lorenz functions. The spectrum for the particles before the CP measurement (Fig. 13a) exhibited only two types of quadrupole splitting. Because the saturation magnetization of the particles at R.T. before the CP measurement was 0.46 Am^2/kg (Fig. 11a), the particles contained ferri- or ferromagnetic compounds. Based on the XRD pattern (Fig. 2), one of these compounds was probably γ-Fe_2O_3(Fe_3O_4), which is a ferrimagnetic compound at R.T. [8]. However, magnetic splitting was not observed due to noise in the spectrum (Fig. 13a). On the other hand, the two types of quadrupole splitting observed in Fig. 13a probably correspond to two paramagnetic compounds, namely, $YFe_{(3+x)}O_{1.5(4+x)}$ and h-$YFeO_3$ (Fig. 2). Because h-$YFeO_3$ is a paramagnetic compound, a single type of quadrupole splitting corresponds to h-$YFeO_3$. The Mössbauer spectrum for the particles after the CP measurement (Fig. 13b) showed magnetic splitting, which could be divided into two Lorenz functions. Based on XRD patterns (Fig. 9), the particles contained $YFe_{(3+x)}O_{1.5(4+x)}$, h-$YFeO_3$, and γ-Fe_2O_3(Fe_3O_4). However, ε-Fe_2O_3 could not be identified in the XRD pattern. The saturation magnetization of the particles at R.T. after the CP measurement was 24.4 Am^2/kg (Fig. 11b). Based

on the Mössbauer parameters (Table 4), the magnetic splitting evident in Fig. 13b corresponds to γ-Fe_2O_3(Fe_3O_4).

The relative quantity of h-$YFeO_3$ to that of $YFe_{(3+x)}O_{1.5(4+x)}$ (XRD pattern in Fig. 9) in the particles after the CP measurement increased compared with that before the measurement. The two types of quadrupole splitting are evident in the Mössbauer spectra for the particles before (Fig. 13a) and after (Fig. 13b) the CP measurement. In one type whose *QS* was small (Table 4), *Area* decreased after the CP measurement, indicating that this type corresponds to $YFe_{(3+x)}O_{1.5(4+x)}$. In contrast, the other type whose *QS* was large, corresponds to h-$YFeO_3$. These results reveal that $YFe_{(3+x)}O_{1.5(4+x)}$ is a paramagnetic compound.

4. Conclusions

The magnetic properties were studied for Y–Fe–O ultrafine particles containing $YFe_{(3+x)}O_{1.5(4+x)}$ synthesized using a thermal plasma evaporation method. The results yield the following conclusions:

(1) After Curie point measurement of the synthesized Y–Fe–O ultrafine particles is conducted under a reduced pressure of 4×10^{-3} Pa from room temperature to either 600 or 700 °C, the relative quantities of h-$YFeO_3$ and γ-Fe_2O_3(Fe_3O_4) to that of $YFe_{(3+x)}O_{1.5(4+x)}$ of the particles (based on the XRD pattern) increase due to a chemical reaction. The relative quantities after the Curie point measurement depend on Fe/Y of the particles.

(2) Saturation magnetization of the particles at room temperature after the Curie point measurement under reduced pressure (4×10^{-3} Pa) increase due to an increase in the relative quantity of γ-Fe_2O_3(Fe_3O_4) in the particles (based on the XRD pattern).

(3) $YFe_{(3+x)}O_{1.5(4+x)}$ in the synthesized Y–Fe–O ultrafine particles is a paramagnetic compound.

References

[1] T. Kanou, H. Yanaghida, Rare earths—properties and applications, Gihoudou Shuttpan, Tokyo, 1980.
[2] M. Douyama, Reametaru Jiten, Fuji Tekunoshisutemu, Tokyo, 1991.
[3] M. Sugasawa, N. Kikukawa, N. Ishikawa, J. Soc. Powder Technol. Jpn. 32 (1995) 660–667 (in Japanese).
[4] M. Sugasawa, N. Kikukawa, N. Ishikawa, N. Kayano, T. Kimura, J. NIRE 6 (1997) 231–240 (in Japanese).
[5] M. Sugasawa, N. Kikukawa, N. Ishikawa, N. Kayano, T. Kimura, Resour. Process. 44 (1997) 74–79 (in Japanese).
[6] M. Sugasawa, N. Kikukawa, N. Ishikawa, N. Kayano, T. Kimura, J. Aerosol Sci. 29 (1998) 675–686.
[7] M. Sugasawa, N. Kikukawa, N. Kayano, T. Kimura, J. Aerosol Res. Jpn. 15 (2000) 264–272 (in Japanese).
[8] M. Sugasawa, N. Kikukawa, Y. Nagano, N. Kayano, T. Kimura, J. Soc. Powder Technol. Jpn. 40 (2003) 720–728 (in Japanese).
[9] M. Sugasawa, N. Kikukawa, Y. Nagano, N. Kayano, T. Kimura, Ceram. Int. (in press).
[10] S. Takeuchi, T. Okada, T. Yoshida, K. Akashi, J. Jpn. Inst. Met. 52 (1988) 711–718 (in Japanese).
[11] V.R. Schrader, G. Büttner, Z. Anorg. Allg. Chem. 320 (1963) 220–234 (in German).
[12] E. Tronc, C. Chanéac, J.P. Jolivet, J. Solid State Chem. 139 (1998) 93–104.
[13] D. Nižňaský, A. Lančok, A. Hutlová, J. Buršík, J.-L. Rehspringer, Int. J. Inorg. Mater. 3 (2001) 479–483.
[14] H. Sano, M. Katada, Mössbauer Bunkougaku, Gakukai Shuttpan Sentaa, Tokyo, 1996.
[15] Powder Diffraction File No. 5-667 PDF, International Center for Diffraction Data, 1960.
[16] Powder Diffraction File No. 48-1548 PDF, International Center for Diffraction Data, 1998.